Deposition of Mesoporous Silicon Carbide Thin Films from $(Me_3Si)_4Sn$: Tin Nanoparticles as in Situ Generated Templates

Chia-Hsin Wang,[†] Wen-Yih Shen,[†] Pei-Sun Sheng,[†] Chi-Young Lee,[‡] and Hsin-Tien Chiu[†,*]

Department of Applied Chemistry, National Chiao Tung University, Hsinchu, Taiwan, 30050, Republic of China, and Department of Materials Science and Engineering and Center for Nanotechnology, Materials Science and Microsystems, National Tsing Hua University, Hsinchu, Taiwan, 30043, Republic of China

Received April 18, 2007. Revised Manuscript Received September 6, 2007

With use of $Sn(SiMe_3)_4$ as the precursor, amorphous SiC_{1+x} thin films with Sn nanoparticles embedded were grown on Si substrates at 923 K by low-pressure chemical vapor deposition. After treatment under hydrogen plasma at 923 K, the Sn nanoparticles in the films were removed by an HF solution and by evaporation at 1423 K. Following the removal of Sn, high-temperature treatments at 1273−1423 K converted the amorphous thin films into mesoporous semiconducting β-SiC thin films with pore sizes 10−100 nm.

1. Introduction

In nature and the laboratory, the morphology and structure of many objects are shaped and altered mainly by phase segregation. Interactions among different domains of the constituents may perform cooperatively as hard and soft templates. The effects can be observed in systems such as the formation of minerals,[1] block copolymers,[2] and nanosized inorganic and organic structures.[3−5] In this report, we wish to discuss how to fabricate mesoporous silicon carbide thin films on silicon substrates based on this methodology. Silicon carbide is an excellent semiconductor material for high-temperature, high-power, and high-frequency applications in harsh environments.[6,7] Recently, many new routes have been developed to prepare silicon carbide nanostructures and thin films. These include solid-state carbothermal reduction of silica, solution-phase sol−gel synthesis and preceramic processes, and various chemical vapor deposition techniques.[3,8−18] Porous silicon carbide thin films on SiC or Si are potentially useful for luminescence and sensing devices.[19,20] To date, electrochemical etching of SiC in $HF_{(aq)}$ is the only method to fabricate it into the porous form.[19−21] However, the route may not be suitable for the fabrication of porous SiC layers onto Si wafers because the high reactivity of Si toward the HF electrolyte would cause preferential dissolution of the substrate.[22] Porous SiC powders prepared by carbothermal reduction are also difficult to integrate into the device fabrication process.[16−18] Clearly, a new method is needed to overcome the difficulty. Here, we demonstrate the integration of a metal-organic chemical vapor deposition (MOCVD) process and a phase segregation strategy to achieve this goal.

* Corresponding author. Fax: 886-3-5723764. Tel.: 886-3-5131514. E-mail: htchiu@faculty.nctu.edu.tw.
† National Chiao Tung University.
‡ National Tsing Hua University.

(1) (a) Brian, J.; Charles, F. K. *J. Sed. Petrol.* **1993**, *63*, 1018. (b) Guillaume, C.; Olivier, B.; Christophe, D.; Michel, A.; Eric, P. V. *Catena* **2005**, *59*, 1.
(2) (a) Muthukumar, M.; Ober, C. K.; Thomas, E. L. *Science* **1997**, *277*, 1225. (b) Förster, S.; Plantenberg, T. *Angew. Chem., Int. Ed.* **2002**, *41*, 688.
(3) Wang, C.-H.; Chang, Y.-H.; Yen, M.-Y.; Peng, C.-W.; Lee, C.-Y.; Chiu, H.-T. *Adv. Mater.* **2005**, *17*, 419.
(4) (a) Huang, C.-H.; Chang, Y.-H.; Lee, C.-Y.; Chiu, H.-T. *Langmuir* **2006**, *22*, 10. (b) Yen, M.-Y.; Chiu, C.-W.; Hsia, C.-H.; Chen, F.-R.; Kai, J.-J.; Lee, C.-Y.; Chiu, H.-T. *Adv. Mater.* **2003**, *15*, 235. (c) Hsia, C.-H.; Yen, M.-Y.; Lin, C.-C.; Chiu, H.-T.; Lee, C.-Y. *J. Am. Chem. Soc.* **2003**, *125*, 9940.
(5) (a) Chen, F.; Liu, M. *Chem. Commun.* **1999**, 1829. (b) Kyotani, T.; Ma, Z.; Tomita, A. *Carbon* **2003**, *41*, 1451. (c) Ramesh, P.; Kishi, N.; Sugai, T.; Shinohara, H. *J. Phys. Chem. B* **2006**, *110*, 130. (d) Vallé, K.; Belleville, P.; Pereira, F.; Sanchez, C. *Nat. Mater.* **2006**, *5*, 107.
(6) Fissel, A.; Schroter, B.; Richter, W. *Appl. Phys. Lett.* **1995**, *66*, 3182.
(7) Spetz, A. L.; Baranzani, A.; Tobias, P.; Lundström, I. *Phys. Status Solidi A* **1997**, *162*, 493.
(8) (a) Shin, Y.; Wang, C.; Exarhos, G. J. *Adv. Mater.* **2005**, *17*, 73. (b) Li, Y.; Bando, Y.; Golberg, D. *Adv. Mater.* **2004**, *16*, 93.
(9) Hatakeyama, F.; Kanzaki, S. *J. Am. Ceram. Soc.* **1990**, *73*, 2107.
(10) Seog, I. S.; Kim, C. H. *J. Mater. Sci.* **1993**, *28*, 3227.
(11) (a) Yajima, S.; Hayasht, J.; Hasegawa, Y.; Iimura, M. *J. Mater. Sci.* **1978**, *13*, 2569. (b) Hasegawa, Y.; Iimura, M.; Yajima, S. *J. Mater. Sci.* **1980**, *15*, 720. (c) Hasegawa, Y.; Okamura, K. *J. Mater. Sci.* **1983**, *18*, 3633.
(12) Kamlag, Y.; Goossens, A.; Colbeck, I.; Schoonman, J. *Chem. Vap. Deposition* **2003**, *9*, 125.
(13) Chiu, H.-T.; Huang, S.-C. *J. Mater. Sci. Lett.* **1993**, *12*, 537.
(14) Pitcher, M. W.; Joray, S. J.; Bianconi, P. A. *Adv. Mater.* **2004**, *16*, 706.
(15) (a) Liu, Q.; Wu, H.-J.; Lewis, R.; Maciel, G. E.; Interrante, L. V. *Chem. Mater.* **1999**, *11*, 2038. (b) Cheng, Q.-M.; Interrante, L. V.; Lienhard, M.; Shen, Q.; Wu, Z. *J. Eur. Ceram. Sci.* **2005**, *25*, 233.
(16) Sonnenburg, K.; Adelhelm, P.; Antonietti, M.; Smarsly, B.; Nöske, R.; Strauch, P. *Phys. Chem. Chem. Phys.* **2006**, *8*, 3561.
(17) Lu, A.-H.; Schmidt, W.; Kiefer, W.; Schüth, F. *J. Mater. Sci.* **2005**, *40*, 5091.
(18) Krawiec, P.; Geiger, D.; Kaskel, S. *Chem. Commun.* **2006**, 2469.
(19) Matsumoto, T.; Takahashi, J.; Tamaki, T.; Futagi, T.; Mimura, H.; Kanemitus. Y. *Appl. Phys. Lett.* **1994**, *64*, 226.
(20) (a) Connolly, E. J.; O'Halloran, G. M.; Pham, H. T. M.; Sarro, P. M.; French, P. J. *Sens. Actuators A* **2002**, *99*, 25. (b) Connolly, E. J.; Timmer, B.; Pham, H. T. M.; Groeneweg, J.; Sarro, P. M.; Olthuis, W.; French, P. J. *Sens. Actuators B* **2005**, *109*, 44.
(21) (a) Shor, J. S.; Grimberg, I.; Weiss, B.; Kurtz, A. D. *Appl. Phys. Lett.* **1993**, *62*, 2836. (b) Rittenhouse, T. L.; Bohn, P. W.; Adesida, I. *Solid State Commun.* **2003**, *126*, 245. (c) Rittenhouse, T. L.; Bohn, P. W.; Hossain, T. K.; Adesida, I.; Lindesay, J.; Marcus, A. *J. Appl. Phys.* **2004**, *95*, 490.
(22) Takazawa, A.; Tamura, T.; Yamada, M. *Jpn. J. Appl. Phys.* **1993**, *32*, 3148.

10.1021/cm0710498 CCC: $37.00 © 2007 American Chemical Society
Published on Web 10/05/2007

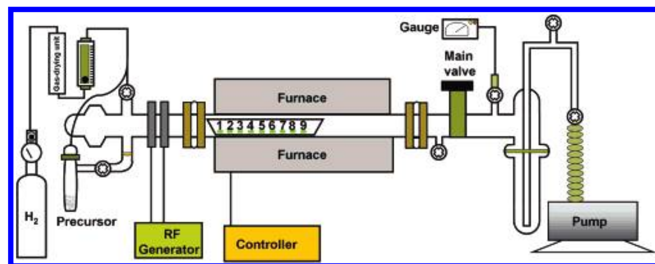

Figure 1. MOCVD reactor setup.

We show that preceramic amorphous SiC_{1+x} thin films containing Sn nanoparticles can be deposited on Si substrates employing $Sn(SiMe_3)_4$ as the precursor. After the Sn nanoparticles are removed, the SiC_{1+x} films are processed further into mesoporous semiconducting β-SiC thin films.

2. Experimental Section

2.1. Materials. The materials used in the present work included trimethylchlorosilane (Aldrich), lithium ribbon (Aldrich, 99.9%), tin(IV) chloride (Aldrich), hydrofluoric acid (Aldrich, 48%), tetrahydrofuran (Echo Chemical, HPLC-grade), acetone (Echo chemical, HPLC-grade), 1,1,1-trichloroethane (Echo Chemical), buffered hydrofluoric acid (BOE) solution (Echo Chemical), n-type silicon (100) wafer (1−10 Ω•cm), and p-type silicon (111) wafer (7−30 Ω•cm). The MOCVD precursor $Sn(SiMe_3)_4$ was synthesized using a literature route.[23]

2.2. Growth of Sn/Amorphous SiC_{1+x} Thin Films, I. The MOCVD experiments were performed in a hot-wall reactor composed of a Lindberg 55342-4 horizontal tube furnace and a 27 mm diameter quartz tube shown in Figure 1. Radio frequency (rf) power (13.56 MHz) was applied to the reactor through two pieces of copper foil electrodes. After the cleaned Si wafers (1 cm × 1 cm) were placed inside the reactor, they were further treated by H_2 plasma (40 sccm, 20 W, 66.7 Pa) at 923 K for 10 min to create a surface favorable to thin film deposition. $Sn(SiMe_3)_4$ (0.5 g) was evaporated into the reactor at 333 K and 26.7 Pa under the assistance of a constant flow of H_2 (20 sccm). The deposition was carried out at 923 K for 6 h to grow dark green thin films (**I**) on the wafers.

2.3. Preparation of Samples I−P, I−P−HF, II, III, and IV. Further processing of **I** by H_2 plasma (20 sccm, 10 W) at 923 K for 6 h followed by dipping into $HF_{(aq)}$ (48%) for 30 min generated **I−P** and **I−P−HF**, respectively. Then, it was annealed at 1273 K for 1 h to produce **II**. On the other hand, **I−P** and **I** were annealed at 1423 K for 1 h to produce **III** and **IV**, respectively.

2.4. Preparation of n-Type β-SiC/p-Type Si Heterojunction. A precursor film **I** was deposited at 923 K for 90 min on p-type Si (7−30 Ω•cm) via the MOCVD process described above. After the film was directly annealed at 1423 K to remove Sn particles embedded inside, **IV** was prepared. P was doped into the film **IV** by ion implantation (5×10^{14} P^{3+}/cm^2 at 25 keV) using a Varian E500HP implanter.

2.5. Characterization. Scanning electron microscopic (SEM) and energy dispersive X-ray (EDX) data were collected using a JEOL JSM-6330F at 15 kV. Transmission electron microscopic (TEM) and selected area electron diffraction (SAED) images were obtained on a JEOL JEM-2010 at 200 kV. Thin films peeled off from the Si wafers either by treating them in $HF_{(aq)}$ or due to poor adhesion were collected for TEM characterizations. X-ray diffraction (XRD) studies were carried out using a Bruker AXS D8 ADVANCE diffractometer using Cu Kα_1 radiation. Fourier transform infrared (FT-IR) spectra were carried out using a Perkin-Elmer Spectrum One. Gas chromatography-mass spectrometry (GC-MS) data of volatile byproducts trapped at 77 K were measured using a HP 5890 series II (GC) coupled to a Micromass TRIO-2000 and a JEOL JMS-D100. On-line residual gas analysis (RGA) was obtained from a VG Quadrupoles Sensorlab 300D mounted to the reactor. Raman spectra of the samples were measured by using a Jabin Yvon T-64000 equipped with an Ar^+ laser (514.5 nm) and a triple monochromator. X-ray photoelectron spectroscopic (XPS) measurements were carried out using a Perkin-Elmer PHI-1600 spectrometer with Mg Kα (1253.6 eV) radiation. Electron probe X-ray microanalysis (EPMA) data were measured from JEOL JXA-8500F. Secondary ion mass spectrometry (SIMS) was carried out using a Cameca IMS-4f instrument.

Connection of Cu wires to the thin films and wafers was made by applying silver paste to form the contacts followed by heating in an oven at 383 K for 30 min. The I−V characteristics of the thin films were measured with a Keithley 2400 (DC ± 5 V) by the two-point probe method. The sheet resistance of the films was determined by the four-point probe method using a CMT-SR 2000 N.

3. Results and Discussion

3.1. Growth and Characterization of Sn/Amorphous SiC_{1+x} Thin Films. The precursor $Sn(SiMe_3)_4$ was vaporized at 333 K into a horizontal hot-wall MOCVD reactor (Figure 1) at 923 K to grow thin films on Si substrates. Starting from the precursor inlet, nine pieces of Si wafers were placed at a distance of 5 cm apart inside the reactor. The substrates were numbered from 1 to 9; the number 1 substrate was at the most upstream position, close to the end of the heated zone, while the number 9 substrate was at the reactor center. Initially, thin films were grown on all of the substrates so that better deposition locations inside the reactor could be chosen. Starting from sample 1, the physical appearance of the films ranged from gray, to dark green with silvery white spots, to dark green, and then to black.

From SEM studies, the morphology and thickness of the films were obtained. From the thickness, the corresponding film growth rates at these positions were estimated to be 0.4−24 nm/min. EPMA and EDX spectra showed that all of the samples contained various amounts of Sn, Si, and C. As shown in the EPMA data in Figure 2, this ranges from 44.5 at. % of Sn, 26.7 at. % of Si, and 28.8 at. % of C for sample 2 to 21.7 at. % of Sn, 33.5 at. % of Si, and 44.8 at. % of C for sample 6. Reliable EPMA data were not collected for samples 1, 7, 8, and 9 because the films were not thick enough to avoid the Si signal from the substrate below. For all samples, XRD studies showed reflections from Sn metal only. This suggests that the metal was phase-segregated from an amorphous composite containing Si and C. Since we wished to employ films with reasonable growth rates, smooth surface, and balanced distribution of Sn and the amorphous Si/C composite, we selected samples 3−5, which were dark green in appearance, for the proposed study. These samples are denoted as sample **I** in the discussion below. This sample and the ones processed from it are summarized in Table 1. The rest of the samples, grown at the positions 1, 2, and 6−9 did not fit the selection criteria for further processing because they were too thin, too high or low in Sn content, and/or contained a high quantity of large-sized particles.

(23) Burger, H.; Goetze, U. *Angew. Chem., Int. Ed.* **1968**, *7*, 212.

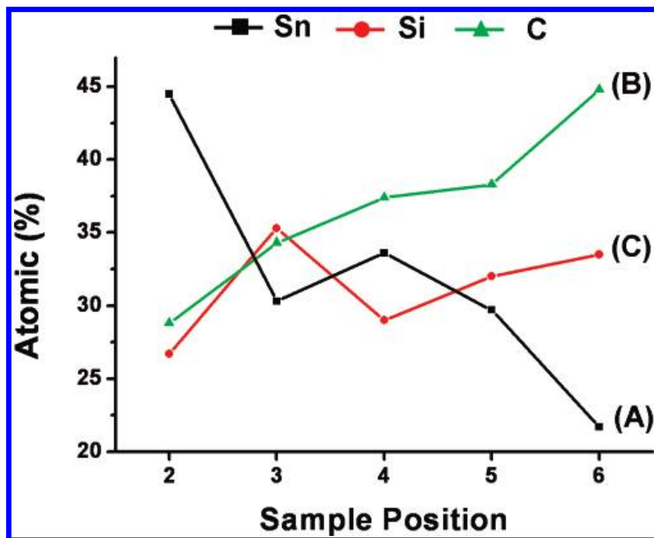

Figure 2. EPMA at. % concentration of the samples grown from $Sn(SiMe_3)_4$ at 923 K, H_2 flow rate 20 sccm, and 26.7 Pa.

The typical surface morphology of **I**, characterized by SEM, is displayed in Figure 3A. The elemental composition of **I**, determined by EDX, is shown in the inset of Figure 3A. It indicates that **I** contains Sn, Si, C, and traces of O. The EPMA data in Figure 2 show that the sample contained 33.6, 29.0, and 37.4 at. % of Sn, Si, and C, respectively. A representative XRD pattern of **I**, as shown in Figure 3B, can be indexed to Sn metal (JCPDS, No. 04-0673).[24] The mean crystallite size of the metal is estimated to be 21.3 nm. This was calculated from the Scherrer equation by using the width data of the Sn(200) reflections. XPS studies showed two binding energies of Sn $3d_{5/2}$ electrons at 486.9 and 484.9 eV. These were assigned to SnO_2 and Sn metal, respectively. The binding energies of Si 2p and C 1s electrons were observed at 100.9 and 283.2 eV, respectively.[25] The data suggest that Si and C atoms formed an amorphous SiC_{1+x} matrix. Since Sn and Si have the same the electronegativity value of 1.8, it is difficult to conclude whether direct Sn−Si bonding existed in the film based on the XPS chemical shift data alone.[26] In the literature, it was reported that the Sn−Si vibration presented a Raman signal near 400 cm^{-1}.[27] For **I**, there was no clear Raman band assignable to this vibration. The FT-IR spectrum of **I** showed a broad absorption peak at 800.2 cm^{-1}, which can be assigned to the Si−C stretching mode. Based on the above information, the film **I** is designated as Sn/amorphous SiC_{1+x} (x = 0−0.3). Even though the as-deposited film contained a significant quantity of Sn, it displayed low electrical conductivity (this will be discussed below in Electrical Property Studies). This intriguing observation suggests that, in **I**, the Sn nanoparticles were dispersed evenly without contacting each other. This morphology would not allow electric current to pass through easily. Otherwise, if the film contained well-connected Sn particles, high electrical conductivity should have been observed.

3.2. Mesoporous Amorphous SiC_{1+x} (x = 2.3) Thin Films. Attempts to remove the Sn nanoparticles by evaporation under low pressure were ineffective at 1273 K but successful at 1423 K. In an alternative approach, we envisioned that by forming channels in **I**, Sn might migrate to the surface for easier removal. This was explored by exposing **I** to H_2 plasma at 923 K. The plasma-treated samples are designated as **I−P**. Indeed, SEM images revealed that numerous spherical Sn particles with a diameter 100−500 nm formed on top of **I−P**. Then, the samples **I−P** were dipped into an HF solution to give samples **I−P−HF**. The SEM image in Figure 4A confirms that the spherical Sn particles were removed. The surface of **I−P−HF** appears to be uneven with randomly distributed spherical pores of 10−50 nm in diameter. The EDX in Figure 4B confirms that the Sn concentration in **I−P−HF** was reduced significantly. In contrast, apparently the other elements were not notably affected. Thus, we conclude that the film **I−P−HF** shown in Figure 4A is porous amorphous SiC_{1+x}.

After **I−P−HF** was annealed at 1273 K, sample **II** was obtained. It displays in Figure 5A basically the same porous surface morphology, without any shrinkage and collapse, as **I−P−HF** does in Figure 4A. An EDX shown in Figure 5B indicates that **II** contains Si, C, and O but without any Sn. EPMA suggested that **II** contained 23.0% Si, 76.9% C, and only 0.1% Sn. The Si/C atomic ratio of **II** was 0.3. In the SEM image shown in Figure 5C, the cross section of **II**, after being removed from the substrate, is displayed. It reveals that the thin film has an average thickness of 3 μm. Figure 5D shows a TEM image of **II** lifted from the wafer. The image reveals that the film contains numerous randomly distributed spherical pores of 10−30 nm in diameter. SAED (inset) reveals that the film is essentially amorphous and does not show any reflection spots from Sn. A FT-IR spectrum of **II** showed a broad absorption at 800.2 cm^{-1}, which can be assigned to the Si−C stretching vibration. This suggests that the processing at 1273 K removed residual Sn to form mesoporous amorphous SiC_{1+x} (x = 2.3) **II**.

3.3. Mesoporous β-SiC Thin Films. Sn nanoparticles can be evaporated successfully from **I** and **I−P** by heating them at 1423 K. In Figure 6, characterization of sample **III**, which was prepared by annealing **I−P** at 1423 K, is presented. In Figure 6A, the SEM image shows a mesoporous film surface with irregular pores of sizes 30−100 nm. The EDX data shown in Figure 6B indicate that **III** contains only Si and C. EPMA showed that **III** contained 42.0% Si, 57.7% C, and only 0.3% Sn. The Si/C atomic ratio of **III** was 0.7. The cross-sectional SEM image shown in Figure 6C reveals that the film thickness of **III** stays at approximately 3.5 μm. After **III** was separated from the wafer, a low-magnification TEM image in Figure 6D shows a projected mesoporous structure with estimated pore spaces 10−80 nm. The SAED image in Figure 6E displays a ring pattern, which can be assigned to the reflections from (111), (220), and (311) planes of polycrystals with a cubic phase. The lattice parameter a is estimated to be 0.435 nm, which is consistent with the

(24) Joint Committee for Powder Diffraction (JCPDS) File No. 04-0673. International Center for Diffraction Data, 1982.
(25) Moulder, J. F.; Stickle, W. F.; Sobol, P. E.; Bomben, K. D. *Handbook of X-ray Photoelectron Spectroscopy*; Physical Electronics: Eden Prairie, MN, 1992.
(26) Zumdahl, S. S. *Chemical Principles*, 2nd ed.; D. C. Heath and Company: Canada, 1995.
(27) Tolle, J.; Chizmeshya, A. V. G.; Fang, Y.-Y.; Kouvetakis, J.; D'Costa, V. R.; Hu, C.-W.; Menéndez, J.; Tsong, I. S. T. *Appl. Phys. Lett.* **2006**, *89*, 231924.

Table 1. Summary of Samples

sample	processing conditions	color	thickness (μm)	pore sizes (nm)	at. %[a] Sn	at. %[a] Si	at. %[a] C	Si/C ratio
I[b]	$Sn(SiMe_3)_4$ decomposed at 923 K, H_2 20 sccm, 26.7 Pa for 6 h	dark green	5.6		33.6	29.4	37.4	0.8
I−P	**I** treated with H_2 plasma at 923 K for 6 h	gray	not measured		not measured	not measured	not measured	
I−P−HF	**I−P** treated with 48% $HF_{(aq)}$ at 298 K for 30 min	black	not measured	10−50[c]	not measured	not measured	not measured	
II	**I−P−HF** annealed at 1273 K under vacuum for 6 h	black	3.0	10−50[d]	0.1	23.0	76.9	0.3
III	**I−P** annealed at 1423 K under vacuum for 1 h	yellow	3.5	10−100[d]	0.3	42.0	57.7	0.7
IV	**I** (grown for only 90 min) annealed at 1423 K under vacuum for 1 h	yellow	0.6	20−100[c]	0[e]	49.8	49.7	1

[a] Atomic ratios were calculated from EPMA data. [b] From position 4 in the reactor. [c] Estimated from SEM image. [d] Estimated from SEM and TEM images. [e] Below detection limit.

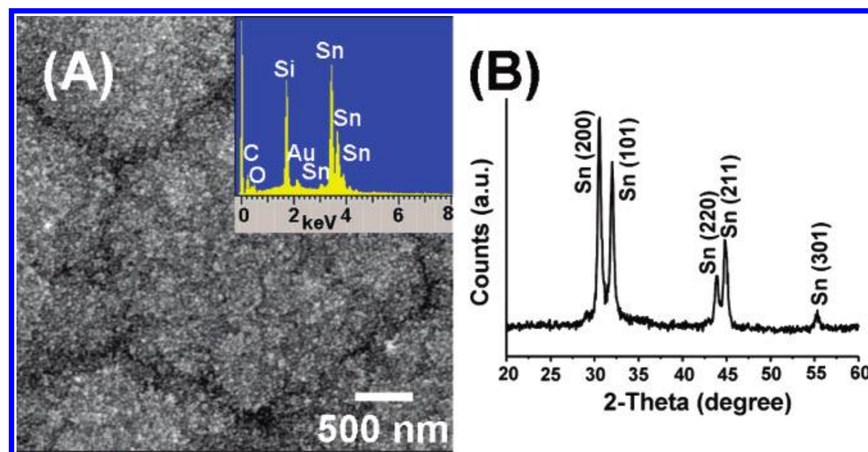

Figure 3. (A) SEM, EDX (inset), and (B) XRD pattern of **I**. **I** was grown from $Sn(SiMe_3)_4$ at 923 K, H_2 flow rate 20 sccm, and 26.7 Pa.

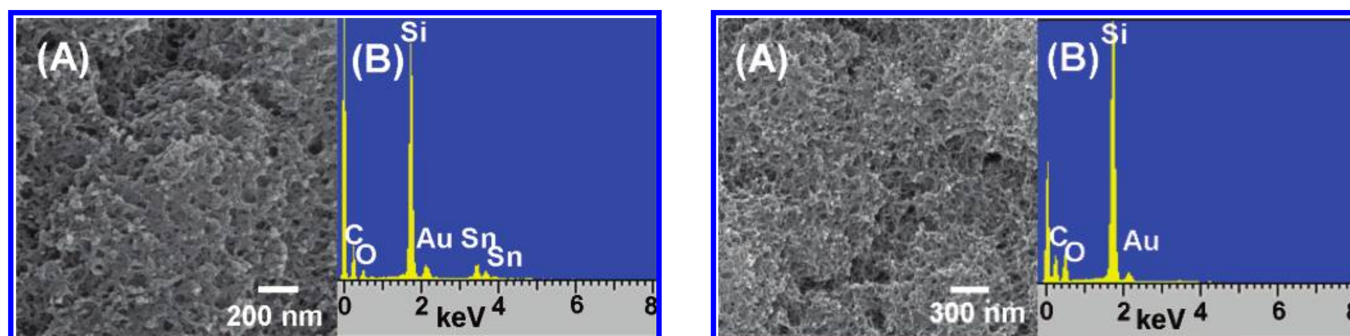

Figure 4. (A) SEM and (B) EDX of **I−P−HF**, prepared by treating **I** with H_2 plasma at 923 K followed by etching in $HF_{(aq)}$ at 298 K.

literature value of β-SiC.[28] A high-resolution TEM (HRTEM) image of the wall of a pore, magnified from the red square in Figure 6D, is shown in Figure 6F. Some fringes spaced at 0.252 nm apart, which originated from the (111) planes of β-SiC, can be observed.[28] In addition, XRD studies also confirmed that **III** was β-SiC.

3.4. Electrical Property Studies. Figure 7 shows the I−V curves derived from electrical characterization of the thin films. **I** reveals a nonconductor type I−V curve in Figure 7A. As the applied bias was swept from −5 to +5 V, the obtained current increased only from −1.4 to +200 μA. This conduction feature is similar to that of well-dispersed metal

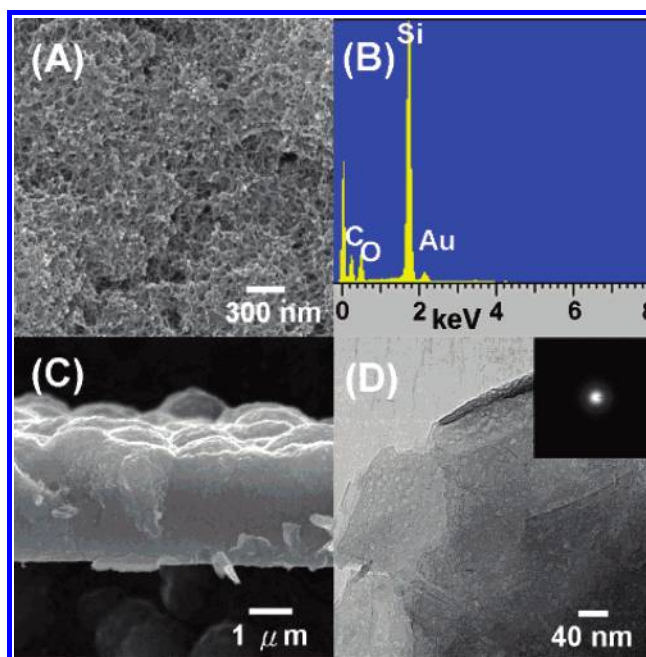

Figure 5. (A) SEM, (B) EDX, (C) cross-sectional SEM, and (D) TEM and ED (inset) of **II**, obtained by annealing **I−P−HF** at 1273 K under vacuum.

nanoparticles, without contacting others, embedded in insulating materials.[29] In Figure 7B, **I−P** annealed at 1073 K

(28) Joint Committee for Powder Diffraction (JCPDS) File No. 29-1129. International Center for Diffraction Data, 1982.

(29) Jin, Y. D.; Cahen, D.; Fridman, N.; Sheves, M. D. *Angew. Chem., Int. Ed.* **2006**, *45*, 6325.

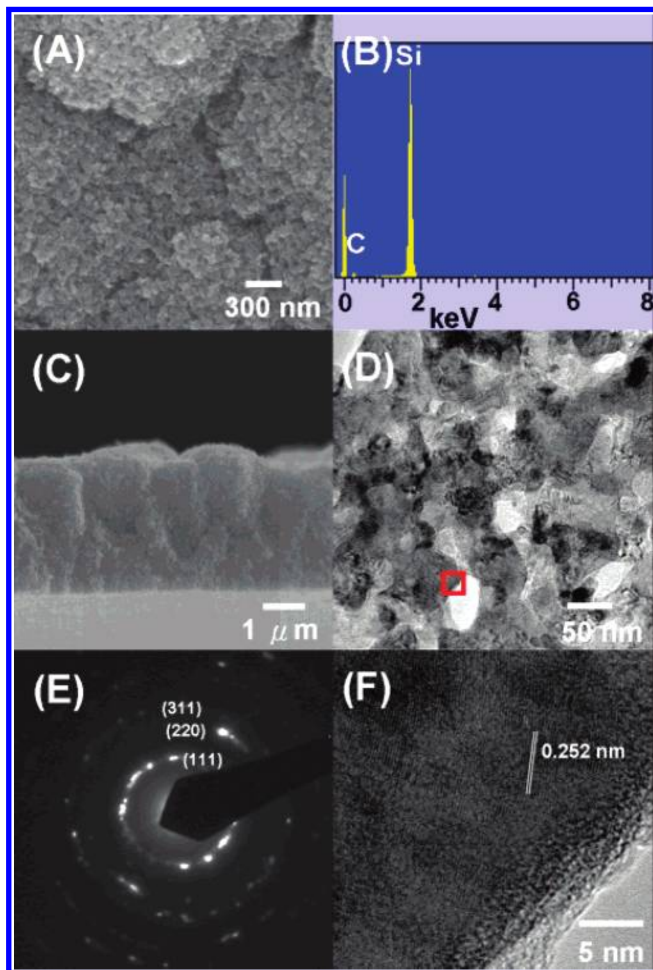

Figure 6. (A) SEM, (B) EDX, (C) cross-sectional SEM, (D) low-magnification TEM, (E) SAED, and (F) HRTEM from the red-square area in (D) of **III**, obtained by annealing **I**−**P** at 1423 K under vacuum.

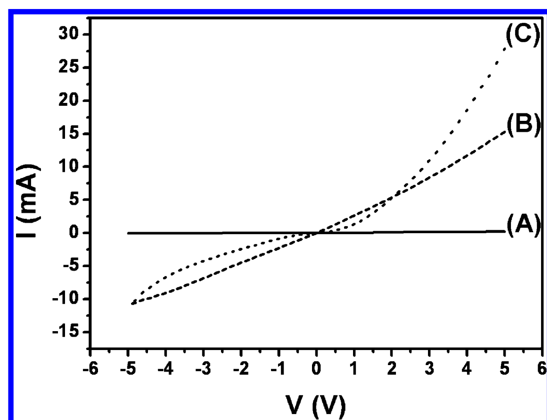

Figure 7. I−V characteristics of (A) **I**, grown from $Sn(SiMe_3)_4$ at 923 K, H_2 flow rate 20 sccm, and 26.7 Pa; (B) **I**−**P** annealed at 1073 K, prepared by treating **I** with H_2 plasma at 923 K and annealed at 1073 K; and (C) **III**, obtained by annealing **I**−**P** at 1423 K under vacuum.

shows a slightly curved I−V feature with an overall resistance of 386 Ω. Since the value is between the values of common metals and insulators, we propose that the Sn particles are loosely connected in this sample. In Figure 7C, **III** shows a nonlinear I−V curve. At an applied bias of ±5 V, the current passing through the junction between the film and the wafer in **III** is 0.1−27 mA. The resistivity, estimated from the sheet resistance, of **III** is 1.03 Ω·cm. This is within the literature values of undoped β-SiC thin films on Si wafers.[30,31]

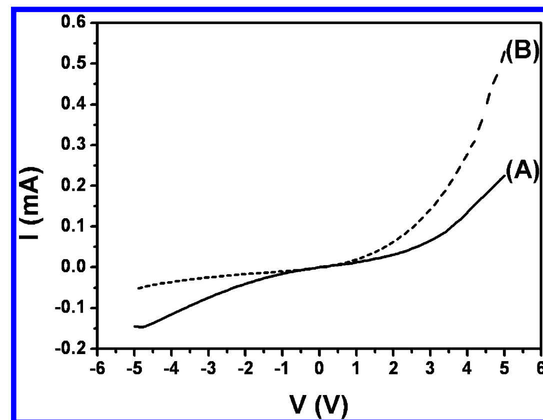

Figure 8. I−V characteristics of (A) **IV**/p-type Si junction and (B) P doped-**IV**/p-type Si junction. **IV** was prepared by annealing **I** (grown for only 90 min) at 1423 K under vacuum for 1 h.

To evaluate potential device applications, P−N junction diodes were fabricated from mesoporous β-SiC films **IV** grown on p-type Si wafers. EPMA showed that **IV** contained 49.8% Si and 49.7% C, which corresponds to the Si/C atomic ratio of 1. The Sn content was below the EPMA detection limit. I−V curves of the devices constructed from undoped and P-doped **IV** are shown in Figures 8A and 8B, respectively. Even though β-SiC is an intrinsic n-type semiconductor, it is obvious that after the film was doped, the n-β-SiC/p-Si heterojunction is significantly improved to show a diode-like rectifying behavior.[32,33] A SIMS depth profile study showed that C, P, and Sn secondary ion concentrations dropped significantly at a depth of ca. 0.6−0.8 μm. This agrees well with the film thickness observed using SEM, 0.6 μm. At the junction, the P atom concentration was ca. 2 $\times 10^{17}$ atoms/cm^3. We suggest that the diode performance was indeed enhanced by the doping process.

3.5. Reaction Pathway Elucidation. Volatile species generated in the MOCVD process were trapped at 77 K and analyzed by GC-MS. The major components were identified to be $HSiMe_3$, Si_2Me_6, and $[Me_2SiCH_2]_2$ (1,1,3,3-tetramethyl-1,3-disilacyclobutane). In addition to these molecules, on-line RGA data suggested that H_2, CH_4, C_2H_2, and C_2H_4, which could not be trapped at 77 K, were also formed in the decomposition process. Since no Sn-containing molecules were detected in the gas-phase byproducts and Sn crystallized into metallic nanoparticles, we propose that the Sn−Si bonds in the precursor $Sn(SiMe_3)_4$ decomposed extensively during the MOCVD process. $Sn(SiMe_3)_4$ might loose $SiMe_3$ radicals sequentially into metastable $Sn(SiMe_3)_3$ and $Sn(SiMe_3)_2$ species and finally into metallic Sn.[13,34] These silyl species,

(30) Gorin, S. N.; Ivanova, L. M. *Phys. Status Solidi B* **1997**, *202*, 221.
(31) Wijesundara, M. B.; Gao, J. D.; Carraro, C.; Howe, R. T.; Maboudian, R. *J. Cryst. Growth* **2003**, *258*, 18.
(32) Muto, H.; Asano, T.; Wang, R.-P.; Kusumori, T. *Appl. Phys. Lett.* **2005**, *87*, 162106.
(33) Furukawa, K.; Vemoto, A.; Shigeta, M.; Suzuki, A.; Nakajima, S. *Appl. Phys. Lett.* **1986**, *45*, 1536.
(34) (a) Wróbel, A. M.; Wickramanayaka, S.; Nakanishi, Y.; Hatanaka, Y.; Pawowski, S.; Olejniczak, W. *Diamond Relat. Mater.* **1997**, *6*, 1081. (b) Wróbel, A. M.; Stanczyk, W. *Chem. Mater.* **1994**, *6*, 1766. (c) Wróbel, A. M.; Wickramanayaka, S.; Nakanishi, Y.; Fukuda, Y.; Hatanaka, Y. *Chem. Mater.* **1995**, *7*, 1403. (d) Wróbel, A. M.;

Scheme 1. Reaction Steps To Form II, Mesoporous Amorphous SiC_{1+x} (x = 2.3) and III, β-SiC Thin Films

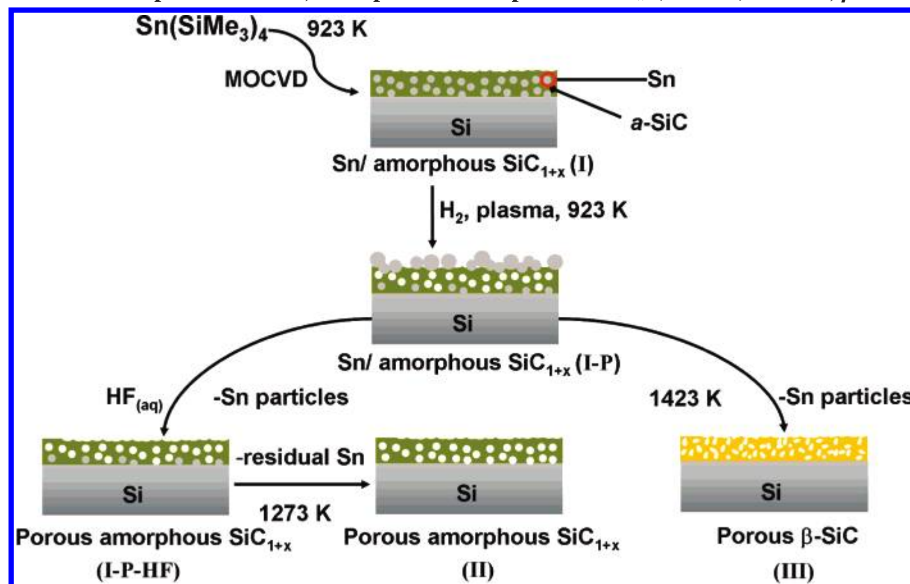

including the $SiMe_3$ radicals evolved and the silane byproducts observed, probably decompose on the substrate surface to deposit the amorphous SiC_{1+x} layer. Due to a large size difference between the elements, the thermodynamic solubility of Sn in Si and C is low.[35,36] For example, thermal decomposition of alkyltin compounds generated elemental Sn and C.[37−39] In this study, the formation of phase-segregated Sn and amorphous SiC_{1+x} is attributed to the same reason. This is in contrast to the solubility of Ge in Si and SiC.[40−42] After the removal of Sn nanoparticles, the amorphous SiC_{1+x} layer was transformed into β-SiC by thermal treatments. The formation of separated Si and C phases was not observed.

The experimental processes performed in this study are shown in Scheme 1. Based on the experimental observations, we suggest that the initially deposited thin film **I** is a composite of sporadic Sn nanoparticles embedded in a preceramic amorphous SiC_{1+x} layer. Then, upon H_2 plasma processing at 923 K, **I** is converted to **I−P**. In the process, **I** is etched to form volatile silanes and hydrocarbons and to leave pores and channels inside the films. These defects would allow fluidic Sn nanoparticles embedded in the preceramic amorphous SiC_{1+x} layer to migrate to the surface easily. The Sn particles would agglomerate into larger ones to reduce the surface tension by ostwald ripening.[43−45] Then, the Sn particles could be removed from **I−P** by dipping it into an HF solution to generate a mesoporous amorphous SiC_{1+x} thin film **I−P−HF**. After the film was annealed at 1273 K under vacuum to evaporate residual Sn, amorphous SiC_{1+x} (x = 2.3) **II** retaining the mesoporous structure is formed. On the other hand, a simple annealing of **I−P** at 1423 K generates porous β-SiC **III** by evaporating Sn particles and crystallizing the SiC component in the film.

4. Conclusions

We have demonstrated a new strategy to fabricate mesoporous silicon carbide thin films by growing a precursor film which contains sporadic Sn nanoparticles embedded in amorphous SiC_{1+x} on Si at 923 K by MOCVD from $Sn(SiMe_3)_4$. The unique phase-segregated film structure is attributed to the low solubility of Sn in SiC. The precursor film can be processed further under hydrogen plasma, in $HF_{(aq)}$, and at high temperature to remove Sn from the deposited layer and convert it into a mesoporous SiC thin film on Si. We also demonstrated how to fabricate p−n junction diodes from the mesoporous n-type SiC thin film on p-type Si wafer. We expect that many unique devices may be developed for future applications.

Acknowledgment. We are grateful for the support from the National Science Council and the Ministry of Education of Taiwan, Republic of China.

Supporting Information Available: Photo images, SEM, EDX, TEM, ED, EPMA, XPS, Raman, FT-IR, XRD, GC-MS, and SIMS (PDF). These materials are available free of charge via the Internet at http://pubs.acs.org.

CM0710498

Walkiewicz-Pietrzykowska, A. *Chem. Vap. Deposition* **1998**, *4*, 133.
(35) Massalski, T. B.; Okamoto, H.; Subramanian, P. R.; Kacprzak, L. *Binary Alloy Phase Diagrams*, 2nd ed.; ASM International: Materials Park, OH, 1990; Vol. 3, p 3361.
(36) (a) Ahn, H.-J.; Kim, Y.-S.; Park, K.-W.; Seong, T.-Y. *Chem. Commum.* **2005**, *1*, 43. (b) Fyhn, M. F.; Chevallier, J.; Larsen, A. N. *J. Vac. Sci. Technol. B* **1998**, *16*, 1777. (c) Min, K. S.; Atwater, H. A. *Appl. Phys. Lett.* **1998**, *72*, 1884.
(37) Margitfalvi, J. L.; Kolosova, I.; Tálas, E.; Göbölös, S. *Appl. Catal. A* **1997**, *154*, L1.
(38) Kim, I.-S.; Blomgren, G. E.; Kumta, P. N. *Electrochem. Solid-State Lett.* **2004**, *7*, A44.
(39) Liu, Y.; Xie, J. Y.; Takeda, Y.; Yang, J. *J. Appl. Electrochem.* **2002**, *32*, 687.
(40) (a) Yonenaga, I. *J. Cryst. Growth* **2005**, *275*, 91. (b) Bolkhovityanov, Yu. B.; Deryabin, A. S.; Gutakovskii, A. K.; Revenko, M. A.; Sokolov, L. V. *J. Cryst. Growth* **2005**, *280*, 309.
(41) Biskupek, J.; Kaiser, U.; Gärtner, K. *J. Electron Microsc.* **2005**, *54*, 493.
(42) Chiu, H.-T.; Shie, C.-S.; Chuang, S.-H. *J. Mater. Res.* **1995**, *10*, 2257.
(43) (a) Wen, H.-C.; Yang, K.; Ou, K.-L.; Wu, W.-F.; Luo, R.-C.; Chou, C.-P. *Microelectron. Eng.* **2005**, *82*, 221. (b) Uh, H. S.; Park, S. S. *J. Electrochem. Soc.* **2004**, *151*, H164.
(44) Zhang, J. H.; Feng, T.; Yu, W. D.; Liu, X. H.; Wang, X.; Li, Q. *Diamond Relat. Mater.* **2004**, *13*, 24.
(45) (a) Weng, C.-H.; Su, H.-C.; Yang, C.-S.; Shin, K.-Y.; Leou, K.-C.; Tsai, C.-H. *Nanotechnology* **2006**, *17*, 5644. (b) Fillot, F.; Tökei, Zs.; Beyer, G. P. *Surf. Sci.* **2007**, *601*, 986.